Korean J. Chem. Eng., 32(5), 974-979 (2015)
DOI: 10.1007/s11814-014-0323-9

pISSN: 0256-1115
eISSN: 1975-7220

Wet chemical synthesis of WO_3 thin films for supercapacitor application

Nanasaheb Madhukar Shinde*,†, Ajay Dattu Jagadale, Vijay Shamrao Kumbhar**, Tanka Raj Rana*, JunHo Kim*, and Chandrakant Dnyandev Lokhande**,†**

*Department of Physics, Incheon National University, 12-1, Songdo-dong, Yeonsu-gu, Incheon 406-772, Korea
**Thin Film Physics Laboratory, Department of Physics, Shivaji University, Kolhapur 416004, India
(*Received 24 August 2014 • accepted 29 October 2014*)

Abstract−Tungstic oxide (WO_3) thin films have been synthesized by wet chemical method, i.e., successive ionic layer adsorption and reaction (SILAR) method. These films are characterized using X-ray diffraction (XRD), scanning electron microscopy (SEM) and optical absorption techniques. The XRD pattern revealed the formation of polycrystalline WO_3 films. Scanning electron micrographs demonstrate the three-dimensional aggregated irregular extended rod shaped morphology of WO_3 thin films. The WO_3 film showed a direct band gap of 2.5 eV. The WO_3 film exhibited specific capacitance of 266 $F \cdot g^{-1}$ in 1 M Na_2SO_4 electrolyte at the scan rate of 10 mVs^{-1}.

Keywords: Wet Chemical Synthesis, SILAR, X-ray Diffraction, Super Capacitor

INTRODUCTION

Supercapacitors are simply capacitors having a superior energy as well as power densities. This capacitance arises either due to electrostatic charge interaction or faradic charge transfer at the electrode-electrolyte interface [1]. There are two types of supercapacitors, depending upon their charge storage mechanism. In the first, charge is stored electrostatically by the reversible and very rapid adsorption and desorption of ions on from high surface area materials known as electrochemical double layer capacitor (EDLC). In the second type, a pseudocapacitor, faradaic reactions occur at the electrode surface and electrons are transferred to valence bands of the redox cathode or anode reagent.

Out of the two types of supercapacitors, pseudocapacitors exhibit a higher capacitance than electric double-layer capacitors (EDLCs). The pseudocapacitors include various transition metal (Ru, Mn, Zn, W, and Ni) oxides and conducting polymer (polypyrrole, polyaniline etc.) materials as working electrodes [2]. Among them, RuO_x and MnO_x based oxides have shown good pseudocapacitive performance. In particular, RuO_x and MnO_x based oxides showed maximum specific capacitances of 768-243 $F \cdot g^{-1}$, respectively. Considering the high cost of RuO_x and MnO_x oxide has been considered as the more suitable of the two metals for practical use as an electrode material in supercapacitors. But low electrical conductivity and poor rate performance of MnO_x pseudocapacitors have been their major demerits. To overcome these drawbacks of RuO_x and MnO_x oxide electrodes, currently novel pseudocapacitors based metal is coming into focus [3].

Recently WO_3 is being used in various fields such as display devices [4], optical smart windows [5], gas-sensors [6], switchable optical [7], catalytic behavior [8], electro chromic [9] and gas chromic [10]. Recently there have been several physical and chemical methods adapted to deposit WO_3 thin films. The physical methods, such as R.F. sputtering [11], pulsed laser deposition (PLD) [12], vacuum evaporation [13] and electron beam [14], are used for deposition of WO_3. On other hand, chemical methods like chemical bath deposition (CBD) [15], sol-gel [16], electrodeposition [17], spray pyrolysis [18] and dip coating [19] are also used for deposition of WO_3 thin films.

Few groups have reported the synthesis of WO_3 thin film by electrodeposition, hard templating and hydrothermal method for supercapacitor application [20-22]. In this investigation, we report for the first time on the wet chemical synthesis of WO_3 thin film, namely successive ionic layer adsorption and reaction (SILAR) method. The WO_3 films are characterized by X-ray diffraction (XRD), scanning electron microscope (SEM), optical absorption techniques, and its supercapacitor behavior is investigated using cyclic voltammetry (CV), galvanostatic charge discharge and impedance measurements.

EXPERIMENTAL DETAILS

1. Preparation of WO_3 Thin Films

The growth of WO_3 thin film was carried out by wet chemical: SILAR method. The 0.1 M H_2O_4W was used as a cationic and 0.01 M NaOH solution was used as an anionic precursor. WO_3 films have been deposited by alternate immersion of stainless steel substrates in 0.1 M H_2O_4W source kept at room temperature (300 K) and 0.1 M NaOH kept at 353 K, respectively. The schematic of the experimental setup for SILAR deposited WO_3 thin film is shown in Fig. 1(a). The photograph of the SILAR unit used for deposition of WO_3 is shown in Fig. 1(b). The visual basic (VB) language based software is used to interface SILAR unit with a computer, which has the ability to control each station of the unit independently, with respect to dipping time, rinsing time and temperature of the bath. Thus, the input parameters for each station include time, rota-

†To whom correspondence should be addressed.
E-mail: nanashinde2009@gmail.com

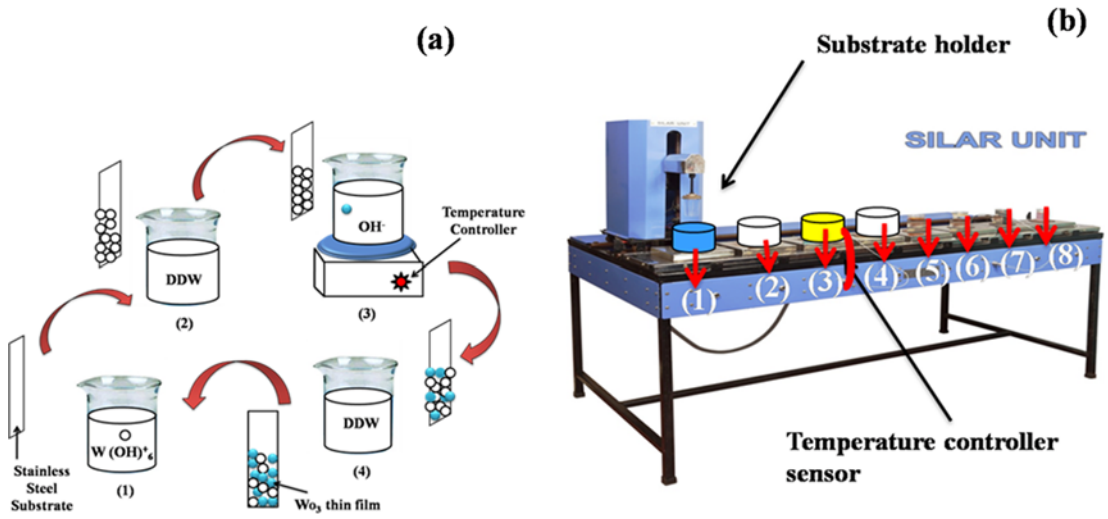

Fig. 1. (a) The schematic diagram of SILAR method for the deposition of WO_3 thin films. Beaker 1st contains cationic precursors of H_2O_4W, beaker 2nd and 4th contain double distilled water (DDW) and beaker 3rd contains anionic precursor of OH^- as NaOH. (b) Actual photograph of computer based SILAR unit.

tion rate and temperature of solution is controlled with help of temperature controller sensor as shown in Fig. 1(b). The adsorption time in cationic solution and reaction time in anionic solution are optimized.

In SILAR method, one SILAR cycle consists of four steps: (1) stainless steel substrate is dipped in the first beaker for 20 s, where adsorption of $W(OH)_6^+$ species takes place, (2) further substrate rinsing in second beaker containing double distilled water (DDW) for 5 s to remove excess adsorbed or loosely bounded $W(OH)_6^+$ species. In step (3), again the substrate is dipped for 10 s in the third beaker containing NaOH precursor solution to form stable WO_3 film and finally step (4), substrate rinsing with DDW for 5 s in the fourth beaker to remove excess or unreacted species or powdery WO_3. The higher concentration of precursor solutions resulted in a higher growth rate, but the quality of the film was poor due to powdery deposit. To remove hydroxide from deposited film and to improve the crystallinity, the films were heat treated at 673 K for 3 h.

2. Characterization Techniques

The crystal structure of the WO_3 thin films was identified by X-ray diffraction analysis using D2 PHASER model purchased from Bruker AXS Analytical Instruments Pvt with Cu (λ=1.5404 Å) target. The surface morphology was visualized using a Model JEOL-6360 scanning electron microscope. The optical absorption study was carried out within a wavelength range of 350-850 nm using a UV-1800 SHIMADZU spectrophotometer with glass substrate as a reference. The cyclic voltametry, and galvanostatic charge-discharge were carried out using (WBCS 3000) automatic battery cycler system. An impedance analyzer (model, CHI6112D) was used to obtain capacitive and resistive parameters in aqueous 1 M Na_2SO_4 electrolyte.

RESULTS AND DISCUSSION

1. Film Formation Mechanism

Thin WO_3 films were obtained by immersing substrate into separately placed cationic and anionic precursors along with rinsing between every immersion with ion exchanged double distilled water. The growth kinetics of a thin film deposition process is ion-by-ion growth mechanism, which involves an ion-by-ion deposition at nucleation sites on the immersed surfaces. According to Lundin and Kitaev, nucleation takes place by adsorption of the colloidal ions and growth occurs as a result of surface coagulation of these ions, giving thin and adherent film [23].

In WO_3 thin film deposition, the film is deposited on a substrate through a controlled heterogeneous precipitation of H_2O_4W. The proposed reaction mechanism is as follows: for deposition of WO_3 films, H_2O_4W was used as a source of tungstic oxide. When ammonia was added to it, a white precipitate occurred, which was dissolved by additional dropwise addition of aqueous ammonia. This can be represented by the following reactions:

$$H_2O_4W+6NH_4OH \rightarrow W(OH)_6^+ +6NH_3 \uparrow +4H_2O \quad (1)$$

In the SILAR method, a thin layer of $W(OH)_6$ ions is adsorbed on the substrate by the immersion of the substrate into the cationic precursor solution kept at room temperature.

The further reaction is followed when the immersion of $W(OH)_6^+$ ions is adsorbed substrate in NaOH anionic solution, where the chemical reaction between OH^- and the adsorbed $W(OH)_6^+$ ions leads to the deposition of adherent WO_3 layer.

$$W(OH)_6^+ \rightarrow WO_3^+ +3H_2O \quad (2)$$

The non-adherent and unbounded particles were washed away into the water bath. The cycle of ion adsorption followed by chemical reaction is repeated several times to achieve terminal film thickness of 0.08 mg·cm^{-2}. Fig. 2 shows the film thickness variation with number of deposition cycles. The rate of increase in the thickness is nonlinear, which has been attributed to the growth by nucleation and coalescence process. More nucleation sites contribute to coagulation during the growing procedure. Furthermore, slight decrease in film thickness observed could be attributed to the formation of

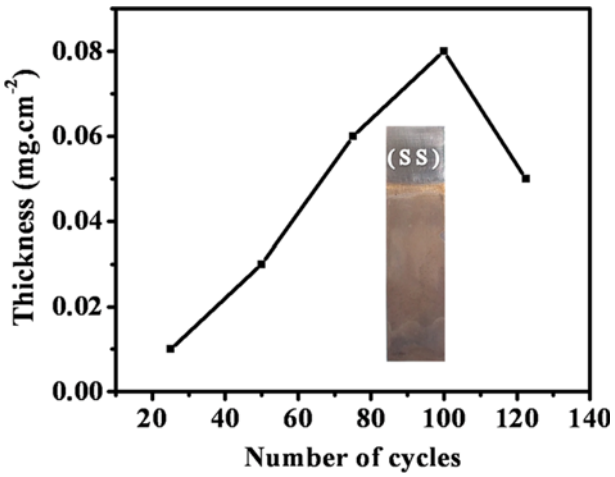

Fig. 2. Variation of WO_3 film thickness with number of cycles. (Inset shows photographs of WO_3 thin films at 0.08 mg·cm^{-2} maximum thicknesses).

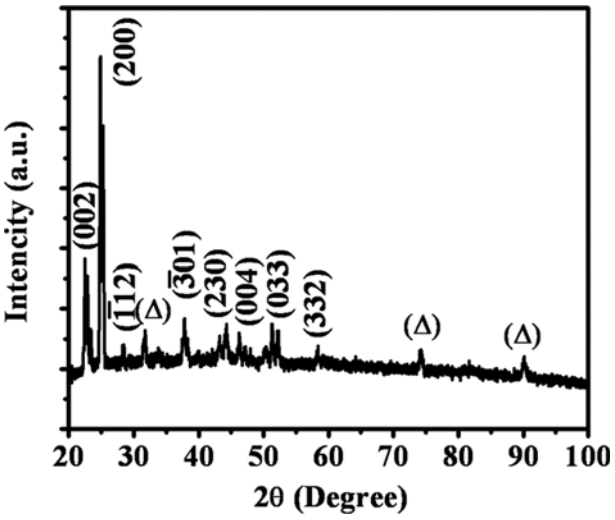

Fig. 3. The X-ray diffraction pattern of WO_3 thin film on glass substrate.

outer porous layer and/or the film, which may develop stress to cause delamination, resulting in peeling off the film after the film reaches at maximum thickness.

2. Structural Studies

Fig. 3 shows a typical XRD pattern of WO_3 thin film. The locations of peaks are corresponding to WO_3 such as (002), (200), ($\bar{1}$12), ($\bar{3}$01), (230), (004), (033) and (332) are in good agreement with JCPDS card no. [71-2141]. In addition, peaks marked with a triangle ('Δ') are assigned to the characteristic peaks of the stainless steel substrate. Thus, a WO_3 thin film has the monoclinic (JCPDS card no. 75-1560) structure with preferential growth of certain plane. Zou et al. [24] reported the monoclinic structure for WO_3 thin films by nonaqueous synthetic route. Similar type of result was also obtained by Hieu et al. [25] in case of WO_3 thin film deposited through thermal method. The grain size of WO_3 thin films from XRD pattern was calculated using the Scherrer relation:

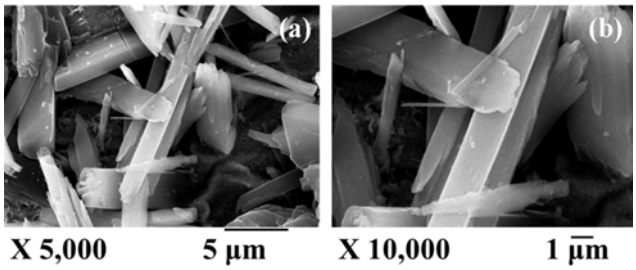

Fig. 4. The SEM images of WO_3 thin film at (a) ×5,000 and (b) ×10,000 magnifications.

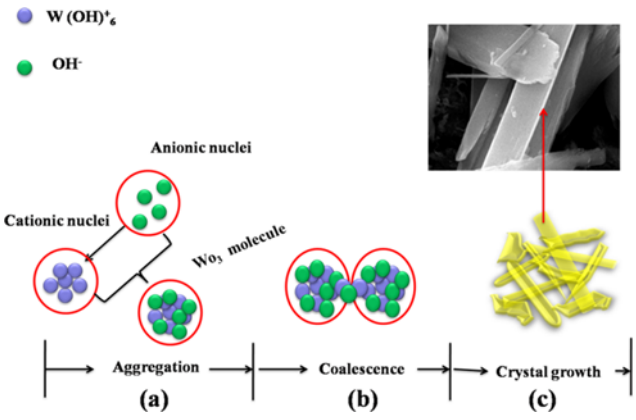

Fig. 5. The schematic representation of growth process of WO_3 thin film (a) aggregation (b) coalescence and (c) crystal growth (Inset shows enlarge SEM image of as deposited WO_3).

$$D = \frac{0.9\lambda}{\beta \cos\theta} \quad (3)$$

where β is the broadening of diffraction line measured at half maximum intensity (radians) and λ=1.5404 Å , the wavelength of the CuKα X-ray. The grain size was found to be 45 nm for (200) plane.

3. Surface Morphology

Fig. 4(a), (b) shows the SEM images of WO_3 thin film at two different magnifications (×5,000 and ×10,000). The total substrate surface was covered uniformly with three-dimensional irregular and aggregated rods with average width of 1-2 μm. These types of rods are electrochemically favorable, since they exhibit high surface area for electrochemical application. Also, their random distribution provides voids for ion movement. Previously, Chang et al. observed rod-like morphology for WO_3 prepared using microwave-assisted hydrothermal synthesis [22]. The schematic of growth mechanism for formation of irregular rod using SILAR method is shown in Fig. 5. Initially, $W(OH)_6^+$ metal ions come closer to each other, resulting in cationic nuclei on the substrate surface. Further from the anionic precursor bath, OH^- ions are adsorbed over the cationic nuclei to form WO_3 molecule in a process called aggregation, as shown in Fig. 5(a). In successive steps, many such WO_3 molecules are merged with each other by means of neck, leading to coalescence as shown in Fig. 5(b). Finally, coalescence process is continuous in different geometric directions and results in formation of irregular rods on substrate surface as shown in Fig. 5(c). Inset shows

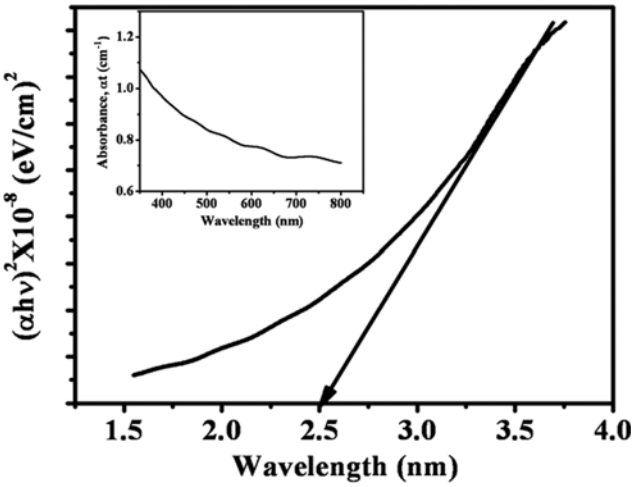

Fig. 6. The variation of absorption (αt) with wavelength (λ) of WO_3 thin film on glass substrate (Inset shows the plot of $(\alpha h\upsilon)^2$ vs. $h\upsilon$ of WO_3 thin film).

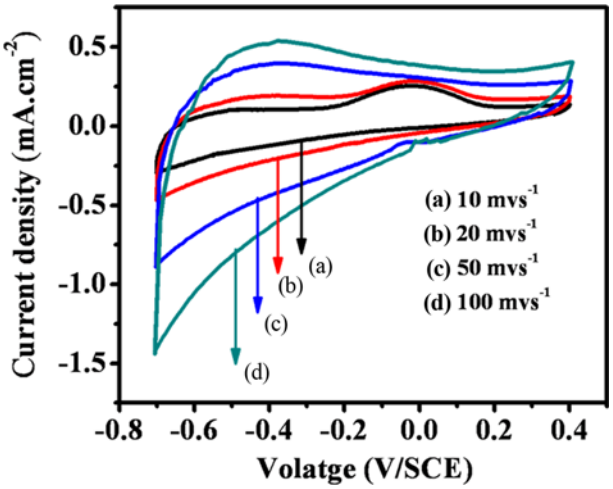

Fig. 7. The cyclic voltammograms of WO_3 thin film at different scanning rates [(a) 10 (b) 20 (c) 50 and (d) 100 mV/s] in the 1 M Na_2SO_4 electrolyte in the −0.7 to +0.4 V Vs SCE.

enlarged SEM image of deposited WO_3 thin film. Similar type of growth mechanism of CdS thin film formation is explained by Hodes et al. [23]. Also, in Lokhande et al., a similar type mechanism was described in case of SILAR deposited CZTS thin film [26].

4. Optical Studies

The optical absorption of WO_3 thin films in the wavelength range 350-850 nm has been investigated. Fig. 6 shows the variation of absorbance (αt) of WO_3 film with wavelength (λ). This spectrum reveals that WO_3 thin film has high absorbance of light in the visible region, indicating applicability as an absorbing material. The optical band gap energy is estimated using the following equation for a semiconductor:

$$\alpha = \frac{A(Eg - h\nu)^m}{h\nu} \quad (4)$$

where α is absorption coefficient, E_g is band gap, A is constant and n is equal to 1/2 for direct transition. Inset of Fig. 6 shows the variation of $(\alpha h\upsilon)^2$ versus $h\upsilon$, which is a straight line in the domain of higher energies, indicating a direct optical transition. The band gap energy, E_g, is obtained by extrapolating the linear portion of the plot $(\alpha h\upsilon)^2$ versus $h\upsilon$ to the energy axis at α=0. From the graph for WO_3 thin film, a band gap value of 2.5 eV is observed, which is consistent with previous reports [27].

5. Supercapacitive Studies

The chemically deposited polycrystalline WO_3 electrodes were used in the supercapacitor and their performance was tested by cyclic voltammogram (CV) technique in 1 M Na_2SO_4 solutions in the potential window of +0.4 to −0.7 V. The electrochemical measurements for supercapacitors were carried out in a three electrode electrochemical cell, in which the WO_3 thin film electrode was used as the working electrode, platinum as the counter, and saturated calomel electrode (SCE) as the reference electrode.

6. CV Study

Fig. 7 shows the CV curves of WO_3 electrode with different scan rates in 1 M Na_2SO_4 electrolyte. The current under the curve slowly increased with scan rate. This shows that the voltammetric currents are directly proportional to the scan rates of CV, indicating an ideally capacitive behavior. The area under curve increases in accordance with double intercalation/deintercalation of both Na^+ and electrons into/out of the WO_3 films following the reaction,

$$WO_3 + xNa^+ \Leftrightarrow xNa^+WO_3 \quad (5)$$

When a negative potential is applied to the WO_3 electrode, electrons and Na^+ ions are inserted into the WO_3 film; the electrons reduce the W^{6+} ions to W^{5+}, whereas the deintercalation of electrons and Na^+ by applying positive voltage results in the W^{5+} ions being oxidized to W^{6+}. Finally, WO_3 undergoes electrochemical charge transfer reactions $W^{6+} \leftrightarrow W^{5+}$ in Na_2SO_4 electrolyte, making it a potential candidate for pseudocapacitor application.

The capacitance (C) was calculated using the following relation:

$$C = \frac{I}{dv/dt} \quad (6)$$

where I is the average current in ampere and dV/dt is the voltage scanning rate.

The interfacial capacitance was calculated using the relation,

$$C_i = \frac{C}{A} \quad (7)$$

where 'A' is the area of active material dipped in the electrolyte.

The specific capacitance Cs (F g^{-1}) of WO_3 electrode was calculated using following relation:

$$C_s = \frac{C}{W} \quad (8)$$

where W is the weight of WO_3 film dipped in electrolyte. The WO_3 electrode exhibited the interfacial capacitance (C_i) of 0.0214 F·cm^{-2} and the specific capacitance (C_s) of 266 F·g^{-1}. The observed values are quite comparable with hydrothermally deposited WO_3 thin films having specific capacitance of 290 F·g^{-1} [27].

Galvanostatic charge-discharge plot measured at 1 mA·cm^{-2} is shown in Fig. 8. The observed non-linearity in charge-discharge

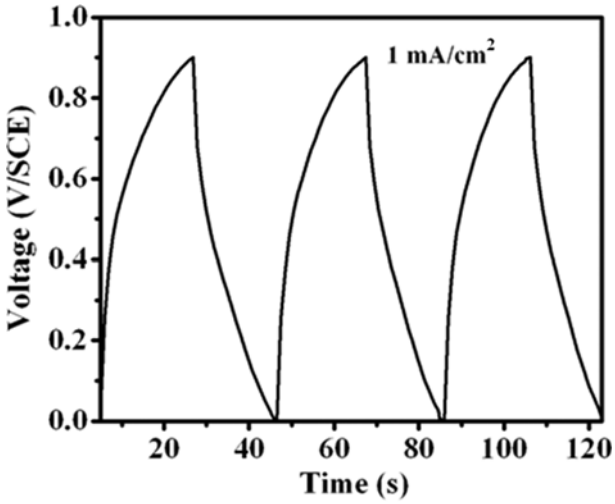

Fig. 8. Galvanostatic charge-discharge curves of WO_3 thin film at 1 mA·cm^{-2} in 1 M Na_2SO_4 electrolyte.

profile, which deviated from the typical linear variation of voltage with time, normally exhibited by an electrochemical double layer capacitor, can be explained as due to the pseudocapacitance arising out of the redox reaction at this voltage range. At the beginning of the charge and the discharge, a sharp change in voltage is due to the equivalent series resistance (ESR) of the electrochemical cell.

The specific energy, power and coulombic efficiency have been estimated from the following equations:

$$\text{Specific enegry : S.E} = \frac{V \times I_d \times T_d}{W} \quad (9)$$

$$\text{Specific power : S.P} = \frac{V \times T_d}{W} \quad (10)$$

$$\text{Coulombic eficiency : } \eta = \frac{T_d}{T_c} \quad (11)$$

where, I_d is discharge current, T_d is discharge time and W is the total mass of WO_3 film material coated onto both of the stainless steel substrates. The electrical parameters, such as specific power (SP), specific energy (SE) and coulombic efficiency (η %) are found to be 10.12 kW·kg^{-1}, 55.68 Wh·kg^{-1} and 92 %, respectively.

7. Stability of Electrode

The cycle life (stability) of WO_3 electrode in 1 M Na_2SO_4 was tested by CV. Fig. 9 shows the CV curves for 1st , 500th and 1000th number cycle. The current under curve is decreased by 81% up to 1000th cycles. The decrement in specific capacitance occurs with the 1000th cycles caused by the loss of active material through the dissolution and/or detachment, during charging/discharging cycles in the electrolyte. We found that our system can withstand about 1000 cycles without a significant decrease in the capacity compared with WO_3 electrode, illustrating the stable nature of WO_3 electrode in energy storage application.

ELECTROCHEMICAL IMPEDANCE ANALYSIS (EIS STUDIES)

Electrochemical impedance spectroscopy was used in the study of sodium ions insertion in a WO_3 film and in addition charge-transfer steps at the WO_3 electrode/Na_2SO_4 electrolyte interface in quantitative manner. Fig. 10 shows the respective Nyquist plot of supercapacitor cell assembly based on the high surface area WO_3 film in the 1 M Na_2SO_4 aqueous solution film electrode using a three-electrode system in the frequency range of 1 Hz –1 M Hz. The figure shows that the cell has a semicircle in the high frequency region and subsequently shows a straight line in the low frequency region. Inset of Fig. 10 shows enlarged part of semicircle in the high frequency region. From this we concluded that the WO_3 is a supercapacitive electrode. The equivalent (ESR) series resistance of is obtained 81 Ω This is due to the combination of ionic resistance of electrolyte, intrinsic resistance of electrode and contact resistance between electrode and current collector [27]. The distorted semicircle involves the parallel combination charge transfer resistance (R_{ct}) and pseudocapacitance (C) due to redox reactions, whereas a line at 45^0 in mid frequency corresponding to diffusion of Na^+ in electrode representing Warburg element (W), which is quite an analogous result

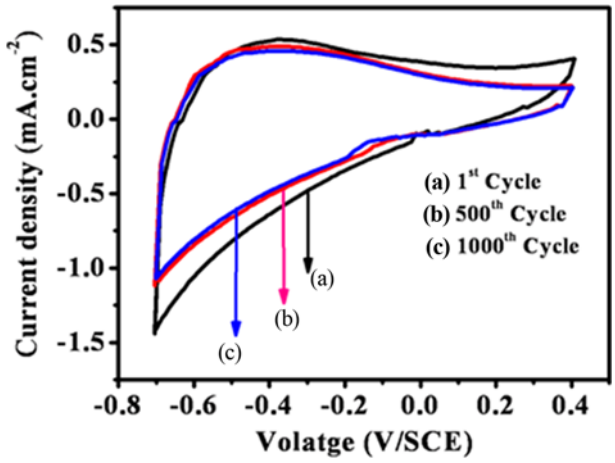

Fig. 9. Electrochemical stability of WO_3 thin film at scan rate of 100 mV s^{-1} at 1st and 1000th cycles in 1 M Na_2SO_4 electrolyte.

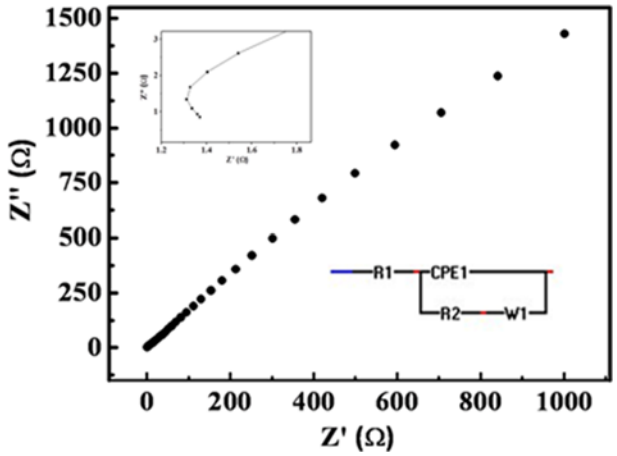

Fig. 10. Nyquist plots obtained for WO_3 electrode in 1 M Na_2SO_4 electrolyte.

Table 1. Fitted parameters for an assumed equivalent circuit

Parameters	R1	R2	w1	P1	n1
Values of the parameters	0.68964 (Ω)	81.702 (Ω)	868.3 ($\Omega \cdot S^{-n}$)	0.0005 ($S \cdot s^{n}$)	0.7318

to impedance spectra of WO_3 recorded in lithium percolate in 1 M propylene carbonate electrolyte [28].

The constant phase element (CPE) is the consequence of non-uniform distribution due to inhomogeneous charge accumulation at electrode surface. This result was also supported the formation of three-dimensional aggregated irregular shape morphology of WO_3 thin films. Kumbhar et al. also observed similar type of result in case of $CoFe_2O_4$ thin film [29]. An equivalent circuit diagram is shown at the bottom of Fig. 10. Table 1 shows fitted parameter for an assumed equivalent circuit, where, CPE1 is the constant phase element, R1 is the solution resistance, R2 is the charge transfer resistance, W1 is the Warburg diffusion resistance, p1 admittance and n is the exponent.

CONCLUSIONS

We have synthesized WO_3 electrodes by wet chemical SILAR method. Under our synthesis conditions, the obtained WO_3 displays three-dimensional aggregated irregular rods shaped morphology providing high surface area, useful for higher charge storage. Subsequently, a high value of specific capacitance (C_s) of 266 Fg^{-1} was obtained. The galvanostatic charge discharge studies show ideal capacitive behavior of an electrode. This has been supported by EIS study. The observed high value of specific capacitance shows that a chemically synthesized WO_3 is a good candidate for supercapacitor application.

ACKNOWLEDGEMENTS

This research was supported by Post-Doctor Research Program (2014) through the Incheon National University (INU), Incheon, South Korea.

REFERENCES

1. B. E. Conway, *Electrochemical Supercapacitors: Scientific Fundamentals and Technological Applications; Kluwer Academics and Plenum*, New York (1999).
2. Y. Wang, Z. Shi, Y. Huang, Y. Ma, C. Wang, C. Chen and M. Chen, Y, *J. Phys. Chem. C.*, **113**, 13103 (2009).
3. S. K. Meher and G. R. Rao, *J. Phys. Chem C.*, **115**, 15646 (2011).
4. K. Hinokuma, A. Kishimoto and T. Kudo, *J. Electrochem. Soc.*, **141**, 876 (1994).
5. C. G. Granqvist, *Handbook of inorganic electrochromic materials, Elsevier, Amsterdam* (1995).
6. S. S. Sunu, E. Prabu, V. Jayaraman, K. I. Gnanasekar and T. Gnanasekaran, *Sens. Actuators, B.*, **94**, 189 (2003).
7. C. G. Granqvist, *Sol. Energy Mater. Sol. Cells*, **60**, 201 (2000).
8. A. Tocchetto and A. Glisenti, *Langmuir*, **16**, 6173 (2000).
9. S. R. Bathe and P. S. Patil, *Smart Mater. Struct.*, **18**, 025004 (2009).
10. L. Zhuang, X. Xu and H. Shen, *Surf. Coat. Technol.*, **167**, 217 (2003).
11. S. S. Kalagi, S. S. Mali, D. S. Dalavi, A. I. Inamdar, H. Im and P. S. Patil, *Electrochim. Acta*, **85**, 501 (2012).
12. F. Mitsugi, E. Hirawa, T. Ikegami, K. Ebihara and R. Kumar, *Jpn. J. Appl. Phys.*, **41**, 5372 (2002).
13. S. Santucci, L. Lozzi, M. Passacantando, S. Nardo and A. Phani, *J. Vac. Sci. Technol. A.*, **2**, 17 (1999).
14. X. Q. Xu, H. Shen and X. Y. Xiong, *Thin Solid Films*, **415**, 290 (2002).
15. Metodija Z. Najdoski and Toni Todorovski, *Mater. Res. Bull.*, **42**, 2025 (2007).
16. Rohini R. Kharade, K. R. Patil, P. S. Patil and P. N. Bhosale, *Mater. Res. Bull.*, **47**, 1787 (2012).
17. B. Yang, H. Li, M. Blackford and V. Luca, *Curr. Appl. Phy.*, **6**, 436 (2006).
18. P. S. Patil, P. R. Patil and E. A. Ennaoui, *Thin Solid Films*, **370**, 38 (2000).
19. M. Deep, T. K. Saxena, D. P. Singh, K. N. Sood and S. A. Agnihotry, *Electrochim. Acta*, **51**, 1974 (2006).
20. X. B. Ren, H. Y. Lu, H. B. Lin, Y. N. Liu and Y. Xing, *Russ. J. Electrochem.*, **46**, 1 (2010).
21. S. Yoon, E. Kang, J. K. Kim, C. W. Lee and J. Lee, *Chem. Commun.*, **47**, 1021 (2011).
22. K. Changa, C. Hu, C. Huang, Ya Liua and C. Ichang, *J. Power Sources*, **196**, 2387 (2011).
23. G. Hodes, *Chemical solution deposition of semiconductor films*, Marcel Dekker, New York, **395**, 40 (2002).
24. X.-X. Zou, G.-D. Li, P.-P. Wang, J. Su, J. Zhao, L.-J. Zhou, Y.-N. Wanga and J.-S. Chen, *Dalton Trans.*, **41**, 9773 (2012).
25. N. V. Hieu, H. V. Vuong, N. V. Duy and N. D. Hoa, *Sens. Actuators, B*, **171**, 760 (2012).
26. N. M. Shinde, P. R. Deshmukh, S. V. Patil and C. D. Lokhande, *Mater. Res. Bull.*, **48**, 1760 (2013).
27. M. Miyauchi, *Phys. Chem. Chem. Phys.*, **10**, 6258 (2008).
28. F. Santiago, G. Belmonte, J. Noem, S. Ferriols, P. Bueno, E. Longo, J. Anto and S. Garc, *J. Electrochem. Soc.*, **7**, 148 (2001).
29. V. S. Kumbhar, A. D. Jagadale, N. M. Shinde and C. D. Lokhande, *Appl. Surf. Sci.*, **259**, 39 (2012).